HAL open science

PSI of the Colonial Alga Botryococcus braunii Has an Unusually Large Antenna Size

Tomas van den Berg, Rameez Arshad, Wojciech Jacek Nawrocki, Egbert Boekema, Roman Kouřil, Roberta Croce

To cite this version:

Tomas van den Berg, Rameez Arshad, Wojciech Jacek Nawrocki, Egbert Boekema, Roman Kouřil, et al.. PSI of the Colonial Alga Botryococcus braunii Has an Unusually Large Antenna Size. Plant Physiology, 2020, 184 (4), pp.2040-2051. ⟨10.1104/pp.20.00823⟩. ⟨hal-04251693⟩

HAL Id: hal-04251693

https://hal.science/hal-04251693v1

Submitted on 20 Oct 2023

HAL is a multi-disciplinary open access archive for the deposit and dissemination of scientific research documents, whether they are published or not. The documents may come from teaching and research institutions in France or abroad, or from public or private research centers.

L'archive ouverte pluridisciplinaire **HAL**, est destinée au dépôt et à la diffusion de documents scientifiques de niveau recherche, publiés ou non, émanant des établissements d'enseignement et de recherche français ou étrangers, des laboratoires publics ou privés.

Autorisation HAL

HAL Authorization

Check for updates

PSI of the Colonial Alga *Botryococcus braunii* Has an Unusually Large Antenna Size[1][OPEN]

Tomas E. van den Berg,[a] Rameez Arshad,[b,c] Wojciech J. Nawrocki,[a] Egbert J. Boekema,[b] Roman Kouřil,[c] and Roberta Croce[a,2,3]

[a]Biophysics of Photosynthesis, Department of Physics and Astronomy-Faculty of Science, Vrije Universiteit Amsterdam, 1081 HV Amsterdam, The Netherlands

[b]Electron Microscopy Group, Groningen Biomolecular Sciences and Biotechnology Institute, University of Groningen, 9747 AG Groningen, The Netherlands

[c]Department of Biophysics, Centre of the Region Haná for Biotechnological and Agricultural Research, Palacký University, 783 71 Olomouc, Czech Republic

ORCID IDs: 0000-0002-7202-4699 (T.E.v.d.B.); 0000-0001-9589-3312 (R.A.); 0000-0001-5124-3000 (W.J.N.); 0000-0001-8211-3348 (R.K.); 0000-0003-3469-834X (R.C.).

PSI is an essential component of the photosynthetic apparatus of oxygenic photosynthesis. While most of its subunits are conserved, recent data have shown that the arrangement of the light-harvesting complexes I (LHCIs) differs substantially in different organisms. Here we studied the PSI-LHCI supercomplex of *Botryococccus braunii,* a colonial green alga with potential for lipid and sugar production, using functional analysis and single-particle electron microscopy of the isolated PSI-LHCI supercomplexes complemented by time-resolved fluorescence spectroscopy in vivo. We established that the largest purified PSI-LHCI supercomplex contains 10 LHCIs (~240 chlorophylls). However, electron microscopy showed heterogeneity in the particles and a total of 13 unique binding sites for the LHCIs around the PSI core. Time-resolved fluorescence spectroscopy indicated that the PSI antenna size in vivo is even larger than that of the purified complex. Based on the comparison of the known PSI structures, we propose that PSI in *B. braunii* can bind LHCIs at all known positions surrounding the core. This organization maximizes the antenna size while maintaining fast excitation energy transfer, and thus high trapping efficiency, within the complex.

The multisubunit-pigment-protein complex PSI is an essential component of the electron transport chain in oxygenic photosynthetic organisms. It utilizes solar energy in the form of visible light to transfer electrons from plastocyanin to ferredoxin.

PSI consists of a core complex composed of 12 to 14 proteins, which contains the reaction center (RC) and ~100 chlorophylls (Chls), and a peripheral antenna system, which enlarges the absorption cross section of the core and differs in different organisms (Mazor et al., 2017; Iwai et al., 2018; Pi et al., 2018; Suga et al., 2019; for reviews, see Croce and van Amerongen, 2020; Suga and Shen, 2020). For the antenna system, cyanobacteria use water-soluble phycobilisomes; green algae, mosses, and plants use membrane-embedded light-harvesting complexes (LHCs); and red algae contain both phycobilisomes and LHCs (Busch and Hippler, 2011). In the core complex, PsaA and PsaB, the subunits that bind the RC Chls, are highly conserved, while the small subunits PsaK, PsaL, PsaM, PsaN, and PsaF have undergone substantial changes in their amino acid sequences during the evolution from cyanobacteria to vascular plants (Grotjohann and Fromme, 2013). The appearance of the core subunits PsaH and PsaG and the change of the PSI supramolecular organization from trimer/tetramer to monomer are associated with the evolution of LHCs in green algae and land plants (Busch and Hippler, 2011; Watanabe et al., 2014).

A characteristic of the PSI complexes conserved through evolution is the presence of "red" forms, i.e. Chls that are lower in energy than the RC (Croce and van Amerongen, 2013). These forms extend the spectral

[1]This work was supported by the Netherlands Organization of Scientific Research (Vici grant to R.C.), the BioSolar Cell Program (grant to R.C., cofinanced by the Dutch Ministry of Economic Affairs), the European Commission Marie Curie Actions Individual Fellowship (grant no. 799083 to W.J.N.), the European Union's Horizon 2020 Research and Innovation Program (grant no. 675006 to R.C., R.A., R.K., E.J.B.), and the European Regional Development Fund project "Plants as a tool for sustainable global development" (project no.CZ. 02.1.01/0.0/0.0/16_019/0000827).

[2]Senior author.

[3]Author for contact: r.croce@vu.nl.

The author responsible for distribution of materials integral to the findings presented in this article in accordance with the policy described in the Instructions for Authors (www.plantphysiol.org) is: Roberta Croce (r.croce@vu.nl).

R.C. conceived the research; T.E.v.d.B., R.A., and W.J.N. performed the experiments; T.E.v.d.B., R.A., and W.J.N. analyzed the data with support from R.K. and R.C.; T.E.v.d.B. and R.C. wrote the manuscript with contributions from R.A. and R.K; and all authors corrected the manuscript and approved the final version.

[OPEN]Articles can be viewed without a subscription.

www.plantphysiol.org/cgi/doi/10.1104/pp.20.00823

Downloaded on December 10, 2020. - Published by https://plantphysiol.org
Copyright (c) 2020 American Society of Plant Biologists. All rights reserved.

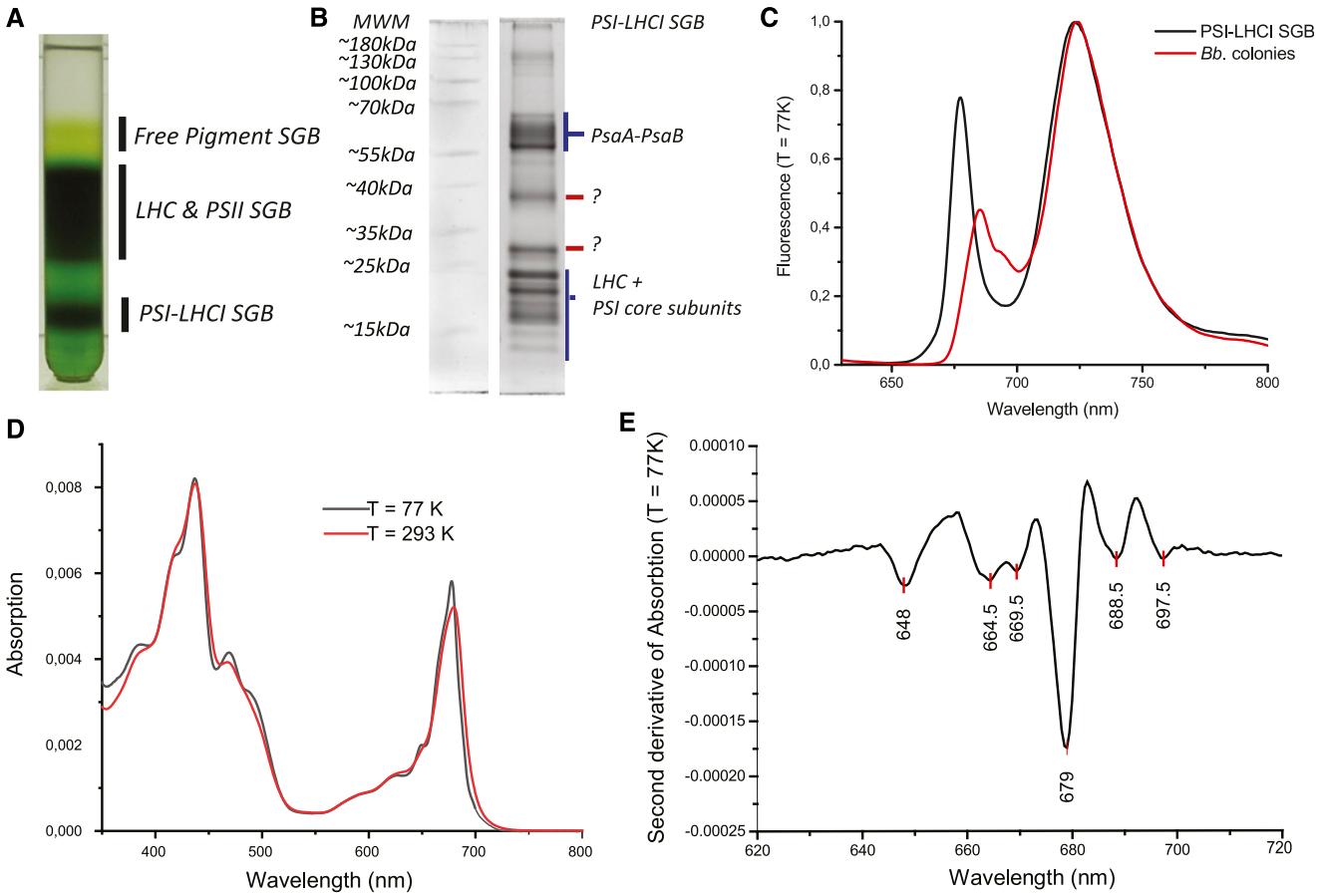

Figure 1. Purification and characterization of *B. braunii* PSI-LHCI supercomplexes. A, Suc density gradient of solubilized thylakoid membranes. The bands were assigned based on their protein content. B, SDS-PAGE of the PSI-LHCI supercomplexes purified by Suc gradient. The bands labeled in red have a M_r not typical for PSI proteins, but they are unidentified due to the absence of the annotated genome. C, Fluorescence emission spectra (440 nm excitation) at 77 K were normalized to the maximum. D, Absorption spectra of the PSI-LHCI supercomplexes at 293 K and 77 K normalized to their integral. E, Second derivative in the Chl Q- region of the absorption spectrum at 77 K. Results were reproduced at least three times on different biological replicas. MWM, Molecular weight marker.

range of PSI beyond that of PSII and contribute significantly to light harvesting in a dense canopy or algae mat, which is enriched in far-red light (Rivadossi et al., 1999). The red forms slow down the energy migration to the RC by introducing uphill transfer steps, but they have little effect on the PSI quantum efficiency, which remains ~1 (Gobets et al., 2001; Jennings et al., 2003; Engelmann et al., 2006; Wientjes et al., 2011). In addition to their role in light-harvesting, the red forms were suggested to be important for photoprotection (Carbonera et al., 2005).

Two types of LHCs can act as PSI antennae in green algae, mosses, and plants: (1) PSI-specific (e.g. LHCI; Croce et al., 2002; Mozzo et al., 2010), Lhcb9 in *Physcomitrella patens* (Iwai et al., 2018), and Tidi in *Dunaliela salina* (Varsano et al., 2006); and (2) promiscuous antennae (i.e. complexes that can serve both PSI and PSII; Kyle et al., 1983; Wientjes et al., 2013a; Drop et al., 2014; Pietrzykowska et al., 2014).

PSI-specific antenna proteins vary in type and number between algae, mosses, and plants. For example, the genomes of several green algae contain a larger number of *lhca* genes than those of vascular plants (Neilson and Durnford, 2010). The PSI-LHCI complex of plants includes only four Lhcas (Lhca1–Lhc4), which are present in all conditions analyzed so far (Ballottari et al., 2007; Wientjes et al., 2009; Mazor et al., 2017), while in algae and mosses, 8 to 10 Lhcas bind to the PSI core (Drop et al., 2011; Iwai et al., 2018; Pinnola et al., 2018; Kubota-Kawai et al., 2019; Suga et al., 2019). Moreover, some PSI-specific antennae are either only expressed, or differently expressed, under certain environmental conditions (Moseley et al., 2002; Varsano et al., 2006; Swingley et al., 2010; Iwai and Yokono, 2017), contributing to the variability of the PSI antenna size in algae and mosses.

The colonial green alga *Botryococcus braunii* (Trebouxiophyceae) is found worldwide throughout different climate zones and has been targeted for the production of hydrocarbons and sugars (Metzger and Largeau, 2005; Eroglu et al., 2011; Tasić et al., 2016).

Downloaded on December 10, 2020. - Published by https://plantphysiol.org
Copyright (c) 2020 American Society of Plant Biologists. All rights reserved.

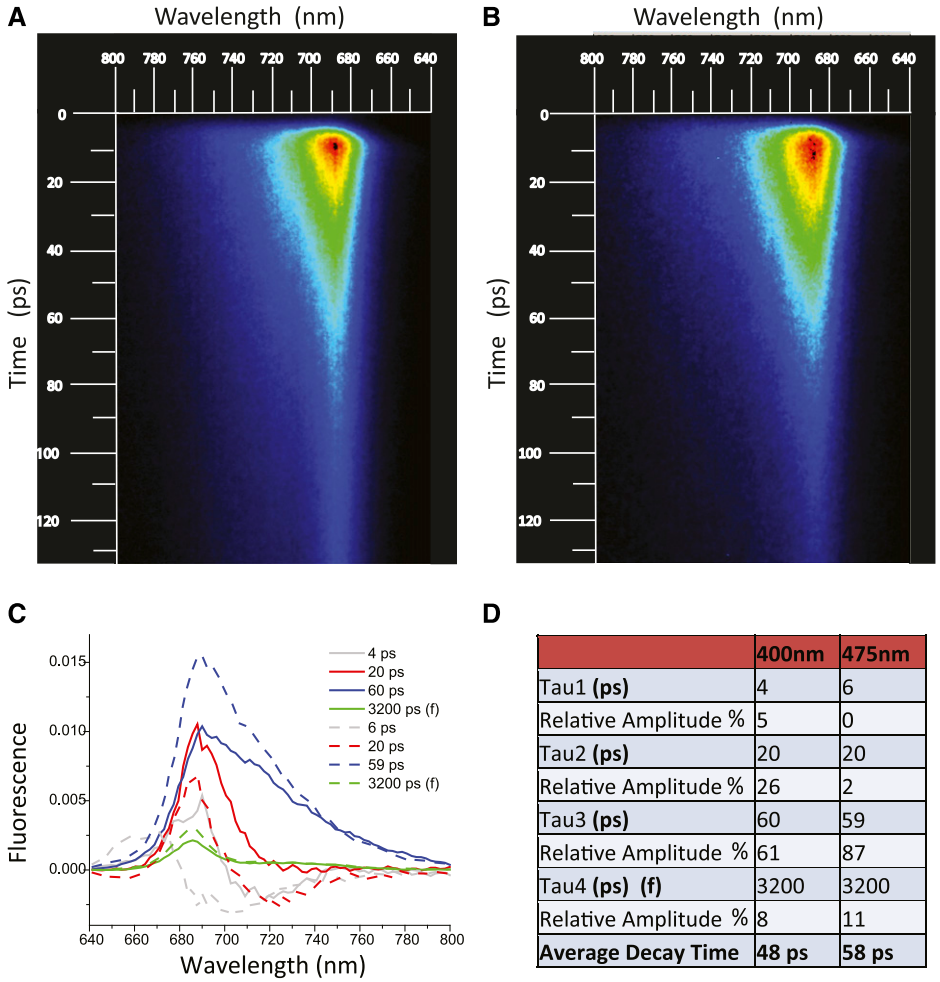

	400nm	475nm
Tau1 **(ps)**	4	6
Relative Amplitude %	5	0
Tau2 **(ps)**	20	20
Relative Amplitude %	26	2
Tau3 **(ps)**	60	59
Relative Amplitude %	61	87
Tau4 **(ps) (f)**	3200	3200
Relative Amplitude %	8	11
Average Decay Time	**48 ps**	**58 ps**

Figure 2. Time-resolved fluorescence of isolated *B. braunii* PSI-LHCI supercomplexes. A and B, Streak camera images of fluorescence of the PSI-LHCI SGB upon 400 (A) and 475 nm (B) excitation. C, DAS of the supercomplexes resulting from the global analyses of the fluorescence decays. Solid lines represent 400 nm excitation and dashed lines 475 nm excitation. The DAS are normalized to the initial excited-state population. D, Lifetimes obtained from sequential analysis of the fluorescence decays of PSI-LHCI supercomplexes measured upon 400 and 475 nm excitation, including relative amplitude and average decay time. Experimental and fit quality are plotted in Supplemental Figure S3. In the Tau4 entry, (f) indicates that the lifetime was fixed at 3,200 ps because the lifetime of this component is hard to estimate at TR1 (140 ps) and the lifetime of *B. braunii* antenna complexes in detergent was previously determined to be 3,200 ps (van den Berg et al., 2018). Measurements at 400 nm excitation were performed on two biological replicas with the same results.

Here, we have purified and characterized PSI from an industrially relevant strain isolated from a mountain lake in Portugal (Gouveia et al., 2017). This *B. braunii* strain forms colonies, and since the light intensity inside the colony is low, it is expected that PSI in this strain has a large antenna size (van den Berg et al., 2019). We provide evidence that *B. braunii* PSI differs from that of closely related organisms through the particular organization of its antenna. The structural and functional characterization of *B. braunii* PSI highlights a large flexibility of PSI and its antennae throughout the green lineage.

RESULTS

PSI core subunits (Supplemental Table S1) were identified in the *B. braunii* genome by similarity searches using query sequences from Arabidopsis (*Arabidopsis thaliana*) and *Chlamydomonas reinhardtii*. The analysis showed that all the PSI core subunits present in these two organisms have clear homologs in *B. braunii* except for PsaN. On the other hand, *B. braunii* contains a gene homologous to *PsaM*, a subunit present in cyanobacteria and red algae but absent in Arabidopsis and *C. reinhardtii*.

To purify the PSI-LHCI supercomplex, the thylakoid membranes of *B. braunii* were mildly solubilized with *n*-dodecyl β-D-maltoside (β-DDM) and loaded on a Suc density gradient. It should be noted that the thylakoid membrane of *B. braunii* is more difficult to solubilize than that of other organisms and that milder detergent conditions do not permit the isolation of PSI-LHCI (see "Materials and Methods"; van den Berg et al., 2018). The band pattern upon centrifugation is shown in Figure 1A. The lower Suc gradient band (SGB) contained PSI-LHCI, as indicated by the presence of the characteristic PsaA-PsaB bands at high M_r and of bands in the region corresponding to the M_r of LHCIs (Fig. 1B). Individual LHCI proteins could not be identified by immunoblot with available LHCI antibodies (van den Berg et al., 2018) or by mass spectroscopy due to the lack of an annotated nuclear genome. The presence of PSI-LHCI in the SGB was confirmed by the absorption and fluorescence emission spectra. The emission spectrum at 77 K (Fig. 1C) had the main peak at 723 nm, which is typical for PSI, while the second peak at 678 nm suggests the presence of contamination with other photosynthetic proteins. The 77 K emission spectrum of the colonies (Fig. 1C) also showed a maximum at 723 nm, indicating that the red-most forms are

Downloaded on December 10, 2020. - Published by https://plantphysiol.org
Copyright (c) 2020 American Society of Plant Biologists. All rights reserved.

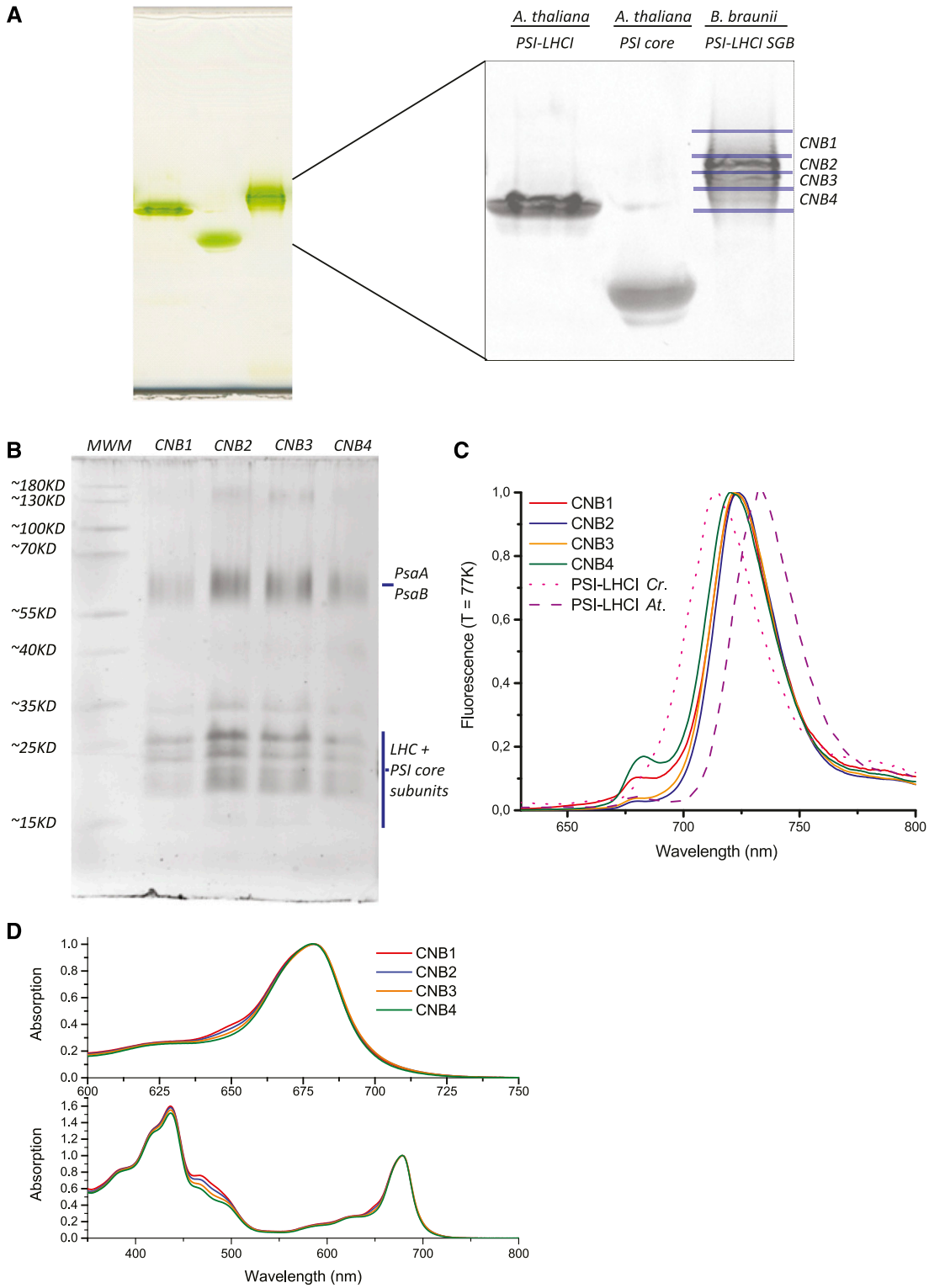

Figure 3. Characterization of subfractions of the *B. braunii* PSI-LHCI Suc gradient band. A, CN gel analyses. The PSI-LHCI SGB of *B. braunii* is compared with the PSI core and PSI-LHCI of Arabidopsis. The inset is a magnification of the CN gel showing the bands that were cut for further analysis. B, SDS-PAGE of the PSI-LHCI supercomplexes eluted from the CN gel. C, Fluorescence emission spectra at 77 K (440 nm excitation) of the *B. braunii* CNBs and PSI-LHCIs from *C. reinhardtii* (*Cr.*) and Arabidopsis (*At.*) colonies normalized to the maximum. D, Absorption spectra at RT of the CNBs normalized to the maximum at 679 nm. Results were reproduced at least three times on different biological replicas.

Downloaded on December 10, 2020. - Published by https://plantphysiol.org
Copyright (c) 2020 American Society of Plant Biologists. All rights reserved.

Table 1. *Pigment composition of the PSI-LHCI supercomplexes*

Values are represented as the mean ± SD of three biological replicas and are normalized to 100 Chls (*a* and *b*). CNB1 to CNB4 are numbered from highest to lowest in terms of M_r. Loro, Loroxanthin; Neo, neoxanthin; Vio, violaxanthin; Lut, lutein; β-car, β-carotene, α-car, α-carotene.

PSI-LHCI	Chl *a*/*b*	Chl/Car	Loro	Neo	Vio	Lut	β-car	α-car
CNB1	4.7 ± 0.5	4.8 ± 0.3	4.8 ± 0.2	1.1 ± 0.2	4 ± 0.1	4.8 ± 0.5	6.6 ± 0.1	1.8 ± 0.1
CNB2	5.6 ± 0.5	4.9 ± 0.2	3.7 ± 0.2	1.4 ± 0.2	4 ± 0.2	5.3 ± 0.2	7 ± 0.9	3 ± 0.9
CNB3	6.6 ± 0.7	4.9 ± 0.2	3.3 ± 0.3	0.6 ± 0.3	4.2 ± 0.2	5.7 ± 0.4	7.5 ± 0.3	3.3 ± 0.3
CNB4	7.6 ± 0.9	4.9 ± 0.3	2.1 ± 1.1	0.5 ± 1.1	4.2 ± 0.1	5.7 ± 0	8.7 ± 0.6	4.3 ± 0.6

preserved in the purified complex. The second derivative of the 77 K absorption spectrum (Fig. 1, D and E) has the red-most minimum at 697.5 nm, which is likely the form responsible for the emission at 723 nm (Fig. 1C). The Stokes shift of 25.5 nm is similar to that of the red forms in Arabidopsis (Romero et al., 2009).

To determine the efficiency of excitation energy transfer and trapping in the PSI-LHCI supercomplex, time and spectrally resolved fluorescence measurements were performed using a streak camera setup. Fluorescence was collected in the 640 to 800 nm range upon preferential excitation of the LHCs (475 nm) or the PSI core (400 nm). Examples of streak camera images are presented in Figure 2, A and B. Four decay components were necessary to obtain a satisfactory fit of the data. The resulting decay-associated spectra (DAS) are shown in Figure 2C. The first component of 4 ps (excitation at 400 nm)/6 ps (excitation at 475 nm) mainly represents excitation energy transfer between Chls *b* and high-energy Chl *a* to low-energy Chls *a*. The second component of 20 ps is a combination of fast trapping (dominating the decay upon 400 nm excitation) and excitation energy transfer from high- to low-energy Chls *a* (dominating decay upon 475 nm excitation). The third component of 60 ps represents the main trapping time. The slowest component has a long lifetime (3,200 ps), a smaller amplitude (8% to 10%), and a maximum at 680 nm, which indicate that it is due to PSII/LHCII contamination (Fig. 2, C and D). Overall, the average fluorescence decay time of isolated PSI-LHCI supercomplexes from *B. braunii* is 48 ps upon 400 nm excitation, and 58 ps upon 475 nm excitation (Fig. 2D), which is 6 ps longer than for *C. reinhardtii* PSI-LHCI (Le Quiniou et al., 2015a).

To determine the M_r of the isolated PSI-LHCI supercomplex, PSI SGB was loaded on a clear native (CN) gel. Four bands (CNB1–CNB4) were separated, one with M_r similar to that of Arabidopsis PSI-LHCI (Fig. 3A) and three with higher M_r. SDS-PAGE confirmed that all four bands contained PSI-LHCI complexes (Fig. 3B). All CN bands exhibit fluorescence maxima at 723 nm (Fig. 3C) except for the lowest band (CNB4), the peak of which was blue shifted 3 nm. The absorption spectra of CNB1 to CNB4 (Fig. 3D) differ in the Chl *b* regions (450–500 nm and 640–660 nm), which show a relative decrease in amplitude going from the largest to the smallest complexes, suggesting differences in the number of LHCIs associated with the PSI core. In agreement with the spectra, pigment analyses show an increase of the Chl *a*/*b* ratio in the smaller PSI-LHCI complexes compared to the larger ones, again indicating differences in the LHCI content (Table 1). The Chl to carotenoid (car) ratio is the same in all complexes, but the CNBs with lower M_r contain less neoxanthin and loroxanthin and more carotenes relative to Chl than the higher-M_r bands (Table 1), again in agreement with a decrease in antenna size. Interestingly, the relative amount of lutein increases in the

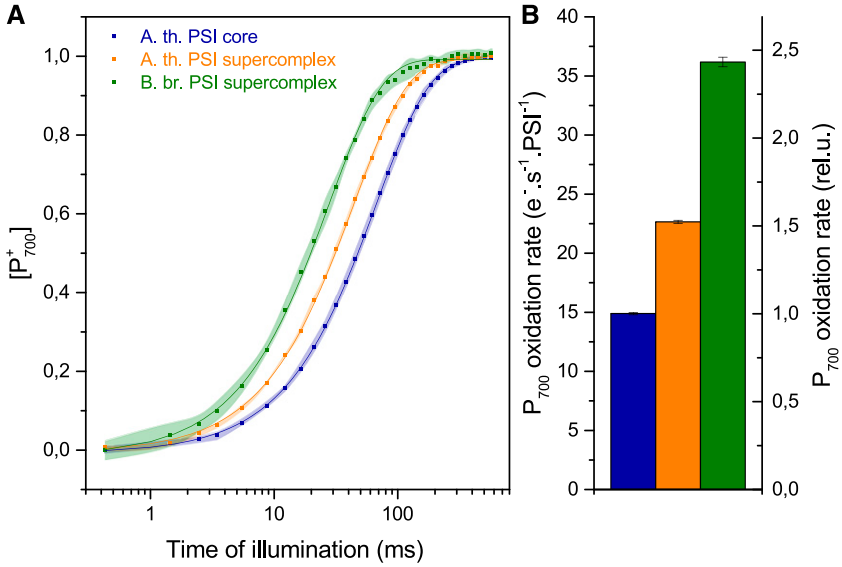

Figure 4. The functional antenna size of the largest PSI-LHCI supercomplex of *B. braunii* (CNB1). A, The kinetics of P_{700} oxidation. Curves were minimum-maximum normalized before averaging and fitting. The points are means of three to six technical replicas in two biological replicas, and the shaded area represents the SD. The solid line is a monoexponential fit of the data. B, Absolute and relative rates of P_{700} oxidation of the samples in A. The rate and SD are parameters of the fit.

Downloaded on December 10, 2020. - Published by https://plantphysiol.org
Copyright (c) 2020 American Society of Plant Biologists. All rights reserved.

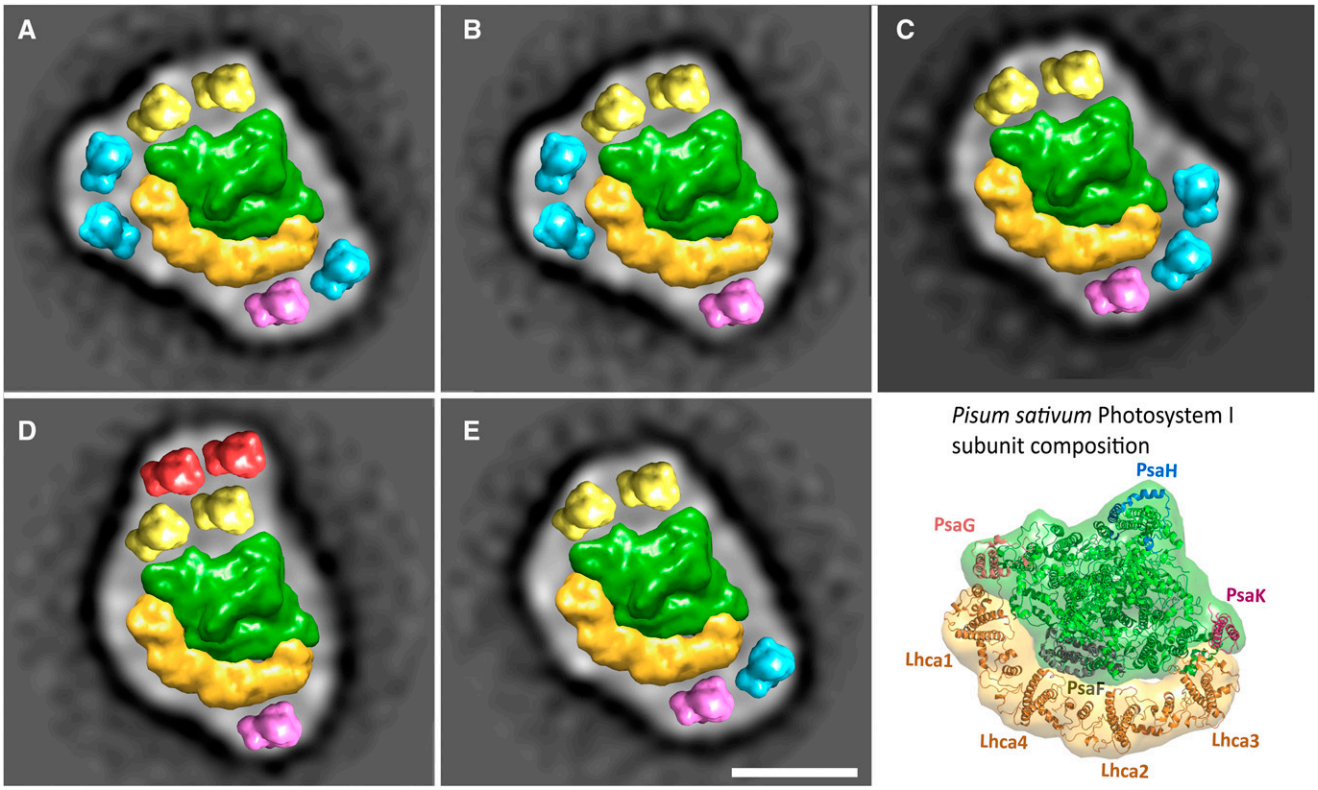

Figure 5. Structural models of PSI-LHCI supercomplexes isolated from *B. braunii* that feature unique antenna positions. A to E, Surface models of the resolved PSI-LHCI supercomplexes from *B. braunii*. The x-ray structure of the plant PSI-LHCI supercomplex (Protein Data Bank 5L8R; Mazor et al., 2017) and the structure of the Lhca1 protein from the same supercomplex were used to fit the EM maps. The PSI core complex is in green. LHCI color codes are as follows: orange, LHCIs that occupy 4 similar positions as in plant PSI-LHCI; yellow, LHCIs binding between PsaG and PsaH; pink, LHCIs binding near Lhca2-3; red, second row of LHCIs binding between PsaG and PsaH; cyan, additional LHCIs. Scale bar = 100 Å.

smaller complexes, suggesting that the LHCI tightly associated with the core contains relatively more lutein than the more loosely bound complexes.

To investigate whether the difference in apparent M_r between *B. braunii* and Arabidopsis PSI supercomplexes (Fig. 3A) results in larger functional antenna size, we measured the P_{700} oxidation kinetics in the largest complex purified (CNB1). Arabidopsis PSI-LHCI complexes were chosen as a control because of their high stability and well-defined antenna size. The kinetics were faster in the CNB1 complex than in PSI-LHCI and the PSI core of plants, which bind 156 and 100 Chls, respectively (Mazor et al., 2017), indicating that the functional antenna size of CNB1 corresponds to ~240 Chls (Fig. 4). This result suggests that 10 LHCIs are associated with the complex (assuming 100 Chls in the PSI core and 14 Chls per LHCI).

To determine the structural organization of the largest purified PSI-LHCI supercomplex, the CNB1 complex was analyzed by single-particle electron microscopy of a negatively stained specimen. CNB1 was preferred over the SGB because of the lower contamination, and especially the absence of Suc. Image analysis of the whole data set resulted in distinct classes of particles. The six major averaged projection maps are shown in Supplemental Figure S2. The structural assignment of each class was obtained by fitting the projection maps with the plant PSI-LHCI structure (Fig. 5; Mazor et al., 2017). The number of bound LHCIs in each particle varies from 8 to 10. The fit indicates that the inner belt of the LHCI proteins contains four complexes, as in the plant PSI-LHCI (Fig. 5, LHCIs in orange), and two additional LHCIs at the PsaG-PsaH side of the core (Fig. 5, yellow). All other LHCIs bind at different positions and form the outer belt. One LHCI, which is present in all projections, is situated on the PsaF-PsaK side (Fig. 5, pink). Others (Fig. 5, cyan) bind to PSI either at the PsaK side (Fig. 5, A, C, and E) or at the PsaG side (Fig. 5, A and B). The final two LHCIs bind on the PsaG-PsaH side (Fig. 5D). Less abundant class averages are shown in Supplemental Figure S3.

Finally, to compare the properties of the purified PSI with that of PSI in vivo, we measured the trapping kinetics of PSI in vivo by time-resolved fluorescence spectroscopy directly on the colonies. The measurements were performed in oxic conditions with the PSII reaction centers closed with 3-(3,4-dichlorophenyl)-1,1-dimethylurea (DCMU) and hydroxylamine (HA; state I),

Downloaded on December 10, 2020. - Published by https://plantphysiol.org
Copyright (c) 2020 American Society of Plant Biologists. All rights reserved.

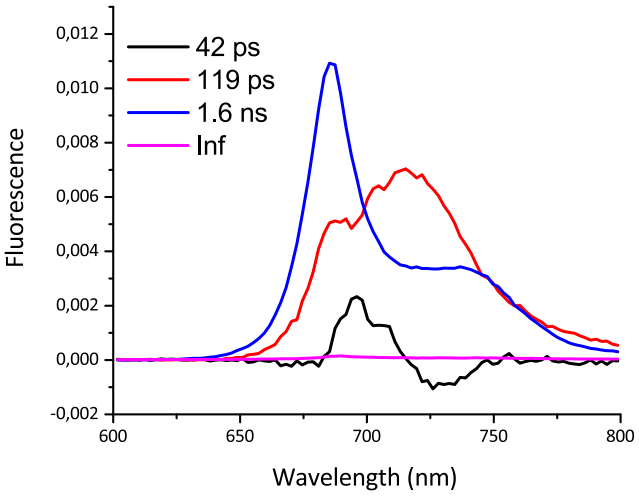

Figure 6. Time-resolved fluorescence of *B. braunii* PSI-LHCI in vivo. The last DAS, (inf), is very small and represents free Chl. Decay time could not be estimated accurately because of the low amplitude and long decay time compared to the largest time window of the experiments (1.4 ns). DAS are normalized against the initial excited-state population. Results were reproduced twice on different biological replicas.

to be able to disentangle the contributions of the two photosystems. The colonies were excited at 400 nm. The data were satisfactorily fitted with four components. The DAS are shown in Figure 6. Based on the spectra, the two main decay components of 119 ps and 1.6 ns can be attributed to PSI and PSII, respectively (Fig. 6). Note that the shape (but not the lifetime) of the PSI DAS in vivo is affected by reabsorption in the colony, similar to what is happening in plants (e.g. Chukhutsina et al., 2019), and therefore cannot be compared directly to that of the isolated complex. The PSI lifetime in the cells is considerably longer than the lifetime of the purified complex (119 versus 48 ps), suggesting that the antenna of *B. braunii* PSI in vivo is larger than that of the isolated complex. An energy transfer component from blue to red forms in PSI is also visible, and its lifetime is longer than in the isolated complex (42 ps versus 20 ps). This indicates that the additional antenna associated with PSI in vivo is less well connected with the rest of the complex. This loose connection has only a small effect on the trapping efficiency (97% versus 94% when considering a lifetime of 2 ns for the nonconnected antenna), but it does not allow us to use the lifetime to determine the exact size of the antenna in vivo, since in this case the lifetime does not scale with the number of pigments.

To estimate the antenna size of *B. braunii*, we then compared the P700 oxidation in the thylakoids of *B. braunii* and Arabidopsis. It was recently shown that in Arabidopsis, 1.4 LHCII trimers are associated with PSI-LHCI in vivo in dark-adapted plants (Chukhutsina et al., 2020). The data (Supplemental Fig. S4) show that also in the thylakoids, the antenna size of PSI in *B. braunii* is larger than in Arabidopsis, suggesting that the antenna of *B. braunii* is composed of ~17 LHC subunits (considering each of them as binding 14 Chls).

DISCUSSION

PSI-LHCI of *B. braunii* Shows a Unique Antenna Organization

In this work we have characterized the PSI-LHCI supercomplex of the colonial green alga *B. braunii*. The largest particle observed contains 10 LHCI proteins associated with the core, as is the case for the PSI-LHCI supercomplex of the green alga *C. reinhardtii* (Ozawa et al., 2018; Kubota-Kawai et al., 2019; Su et al., 2019), but the organization of the LHCIs differs. Moreover, in *B. braunii*, in addition to the complex containing 10 LHCIs, several other PSI-LHCI particles with a different number and organization of LHCIs were observed by electron microscopy. In total, the LHCIs were found to occupy 13 positions (Fig. 5). The four LHCIs in the inner belt are present in the PSI-LHCI of all plants and algae studied so far. Three more are in the outer belt observed in *C. reinhardtii* PSI-LHCI (Fig. 7A), corresponding to *C. reinhardtii* Lhca2, Lhca9, and Lhca5 (Suga et al., 2019). The additional LHCIs positioned on the PsaK side (Fig. 7B) and two of those on the PsaG side (Fig. 7C) largely overlap with the LHCIs observed in the structures of *P. patens* PSI-LHCI (Iwai et al., 2018; Pinnola et al., 2018). The final two LHCI positions in the outer belt on the PsaA side (Fig. 7D, red) are unique to *B. braunii*.

Although we cannot exclude that some of the small PSI-LHCI supercomplexes occur in vivo (Fig. 5), the different particles observed by electron microscopy (EM) are likely the result of a partial disassembly of the PSI-LHCI during purification. In addition, the time-resolved data show that the lifetime of PSI in the cells is far longer than that of the purified complexes (120 versus 48 ps), which indicates that the PSI antenna size is larger in vivo. Note that this is not the result of acclimation to low light as is the case for *P. patens* (Iwai and Yokono, 2017; Iwai et al., 2018; Pinnola et al., 2018), because in *B. braunii* the PSI antenna size remains identical under both low- and high-light growing conditions (van den Berg et al., 2019). Because PSI antenna size does not acclimate to the light intensity, it is also unlikely that PSI antenna size heterogeneity exists in the colony. It is also improbable that this difference in lifetime is due to state transitions, since the colonies were measured in the presence of oxygen with the PSII RCs closed with DCMU and HA, resulting in an oxidized plastoquinone pool, a condition that induces state I in *C. reinhardtii* (Nawrocki et al., 2016). The presence of red forms, which are known to slow down the excitation energy transfer (Jennings et al., 2003; Wientjes et al., 2011; Le Quiniou et al., 2015b), can also not be at the basis of the observed difference between the lifetimes in vivo and in vitro since the red Chl properties are similar in the purified complex and in the cells. The

Downloaded on December 10, 2020. - Published by https://plantphysiol.org
Copyright (c) 2020 American Society of Plant Biologists. All rights reserved.

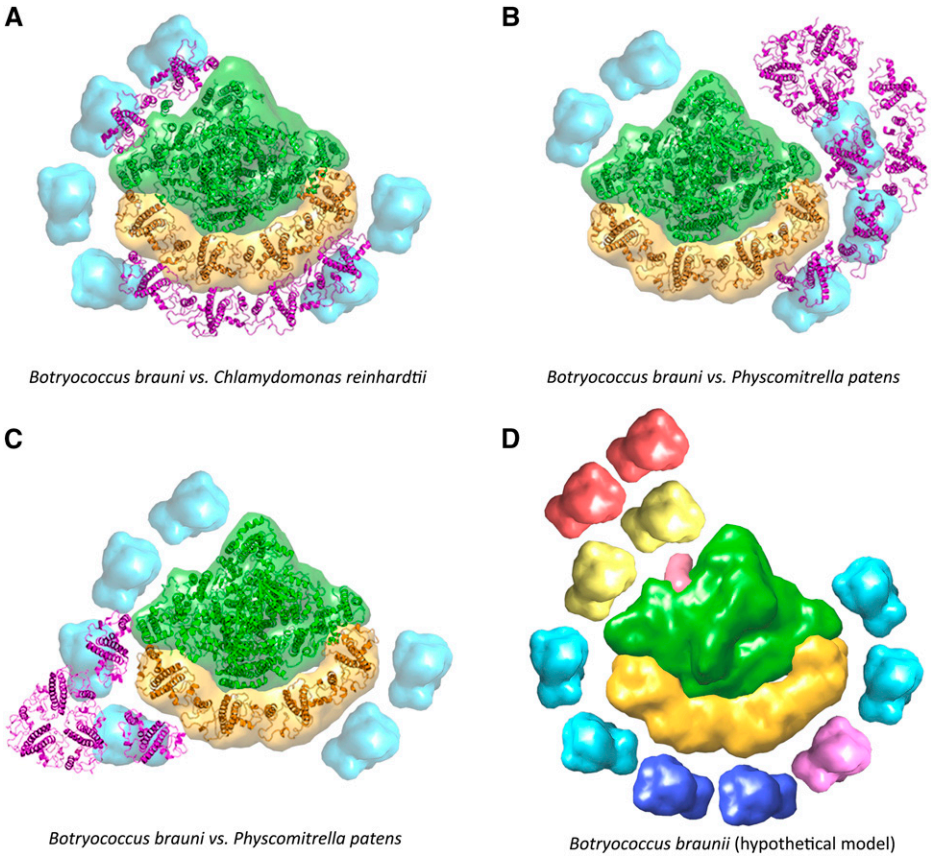

Figure 7. Comparison of a model of the PSI-LHCI supercomplex of *B. braunii* with known PSI structures from other organisms. A, Overlap between the *B. braunii* PSI-LHCI supercomplex from Figure 5A (cyan LHCI) and the PSI-LHCI supercomplex of *C. reinhardtii* (magenta LHCI; Suga et al., 2019). B and C, Overlap between the *B. braunii* PSI-LHCI supercomplex from Figure 5C (cyan LHCI) and the PSI-LHCI supercomplex of the moss *P. patens* (magenta LHCI; Iwai et al., 2018), C, Overlap between the *B. braunii* PSI-LHCI supercomplex from Figure 5A (cyan LHCI) and the PSI supercomplex of *P. patens* (magenta LHCI; Pinnola et al., 2018). D, Hypothetical model of the largest PSI-LHCI supercomplex of *B. braunii*. The model includes (1) the PSI core complex (green), taken from Mazor et al. (2017), and the four Lhca proteins (orange); (2) the position of PsaM (salmon), based on the findings of Qin et al. (2019); (3) additional LHCIs at the binding sites revealed in our study, with new positions (red) or positions similar to those in the PSI of *P. patens* and *C. reinhardtii* (cyan, yellow, and pink); and (4) hypothetical positions of additional LHCIs in vivo, which might occupy empty binding sites in the second belt (blue).

longer lifetime thus indicates that additional complexes are associated with PSI in vivo, increasing its antenna size. This additional antenna is transferring energy relatively slowly to the rest of the complex, indicating that it is less well connected with it than the antenna present in the purified complex. The loose functional connection is probably associated with a weaker structural interaction, which may explain why this part of the antenna is lost during purification. The fact that the purified PSI particle is smaller than the complex in vivo is not surprising, since purification can easily lead to loss of part of the antenna complexes. For example, the largest plant PSI complex purified so far only binds one LHCII trimer (Pan et al., 2018), whereas it is known that PSI binds more LHCIIs in the membranes (Benson et al., 2015; Bos et al., 2017; Chukhutsina et al., 2020). The same holds true for PSII, where the largest purified complex (C2S2M2; Su et al., 2017; Shen et al., 2019) only contains two LHCII trimers per core complex, while in vivo this number is larger and goes up to five (Anderson et al., 1995; Wientjes et al., 2013b).

It is tempting to speculate that all the LHCI positions observed in the different particles are occupied in vivo and that in *B. braunii* the PSI core is surrounded by two belts of LHCIs. This hypothetical model is presented in Figure 7D. Out of the 15 LHCIs shown in this model, 13 were observed in *B. braunii*, whereas the two in the outer belt on the PsaF side were observed in other organisms (Qin et al., 2019; Su et al., 2019) and might have been lost during purification in our study. In this model, the PSI core is surrounded by LHCIs, except at the PsaH/A side, which in plants and *C. reinhardtii* is the docking site for a LHCII trimer in state II (Drop et al., 2014; Pan et al., 2018).

The resulting PSI-LHCI complex is thus expected to have a larger antenna size than those of other green algae. In contrast to unicellular algae, colonial algae

Downloaded on December 10, 2020. - Published by https://plantphysiol.org
Copyright (c) 2020 American Society of Plant Biologists. All rights reserved.

have to deal with constant internal shading by other cells in the colony (Beardall et al., 2009). The optical density of the colonies can be very high, and a large antenna system seems thus essential for the cells in the interior of the colony (van den Berg et al., 2019). In contrast to *B. braunii* hydrocarbon-producing strains, which often float near the water surface and experience high light intensities (Wake and Hillen, 1980), the extracellular polysaccharide (EPS)-producing strain used in this work does not float (Gouveia et al., 2017), and it grows faster under lower light regimes (García-Cubero et al., 2018), in an environment where a large antenna is beneficial. In this respect, it is important to note that our results show that despite the very large antenna, energy trapping in PSI-LHCI remains highly efficient.

Evolution of the PSI Supercomplex from Green Algae to Plants

Recently, several structures of PSI-LHCI complexes from various eukaryotic organisms have been resolved. The basic PSI unit, which corresponds to the PSI of vascular plants, is composed of the core and the four LHCIs located on the PsaG-PsaK side, and is conserved in all the green line organisms analyzed so far (Alboresi et al., 2017; Iwai et al., 2018; Pi et al., 2018; Pinnola et al., 2018; Kubota-Kawai et al., 2019; Qin et al., 2019; Su et al., 2019; Suga et al., 2019). The most striking structural difference between the PSI-LHCI structure of plants and algae/mosses is the presence of a second LHCI belt. In *C. reinhardtii*, Lhca5 was suggested to be essential for connecting the inner and the outer ring of LHCIs (Ozawa et al., 2018) and facilitating excitation energy transfer (EET) between the rings (Suga et al., 2019). Interestingly, this is the only LHCI position in the second belt that is conserved in *P. patens* (Iwai et al., 2018; Pinnola et al., 2018) and in multiple other algal PSIs (Qin et al., 2019; Su et al., 2019; Suga et al., 2019). Thus, Lhca5 might be a structural determinant for the association of the second belt, and it was possibly lost in vascular plants that instead favor a smaller PSI-LHCI complex (Neilson and Durnford, 2010). The binding affinity of Lhca2 and Lhca9 to the core is weak in *C. reinhardtii* (Drop et al., 2011; Su et al., 2019; Suga et al., 2019) but strong in *Bryopsis corticulans* (Qin et al., 2019) and *B. braunii*, as suggested by the fact that these positions are occupied in all the observed particles. This difference may be due to the presence of PsaM (Fig. 7D, pink), which in *B. corticulans* is located in the proximity of Lhca 2 and Lhca9 (Qin et al., 2019) and is present in *B. braunii* but not in *C. reinhardtii*.

In conclusion, the results reported here show the high complexity and diversity in the composition and organization of the PSI antenna in algae. It is worth noting that PSI can afford a large antenna exactly because the extremely fast trapping time assures a very high quantum efficiency (Croce and van Amerongen, 2020).

MATERIALS AND METHODS

Genomic Analyses of PSI in *Botryococcus braunii*

Query sequences from Arabidopsis (*Arabidopsis thaliana*) and *Chlamydomonas reinhardtii* (Supplemental Table S1) were obtained from the UniProt database and used for similarity searches with the BLASTP tool at the National Center for Biotechnology Information in the *B. braunii* genome (not annotated; Browne et al., 2017). The presence of homologs in the *B. braunii* genome was accepted at *E*-values $<10^{-5}$ and/or Bit scores >45.

Isolation and Purification of PSI Supercomplexes from *B. braunii*

B. braunii strain CCALA778 was obtained from the Culture Collection of Autotrophic Organisms and cultured in 1 L modified CHU-13 medium (van den Berg et al., 2018) in 2 L Erlenmeyer flasks, bubbled with 5% (v/v) CO_2-enriched air and shaken at 150 rpm under continuous illumination with white fluorescent light of 15 μmol photons m^{-2} s^{-1}. The culture was harvested in the logarithmic growth phase, and thylakoids were prepared as described previously (van den Berg et al., 2018). Solubilization with digitonin did not work on the *B. braunii* thylakoid membranes and established protocols for styrene-maleic acid copolymer did not yield usable membranes. α-DDM solubilization of the *B. braunii* thylakoid membranes yielded the same Suc band pattern as β-DDM solubilization, but with lower yield and more contaminating proteins. Therefore, mild β-DDM solubilization was used. To purify PSI-LHCI supercomplexes, thylakoids were solubilized at a Chl concentration of 2 mg mL^{-1} with 0.5% β-DDM (w/v) in 400 mM NaCl and 20 mM Tricine-NaOH (pH 7.8) for 20 min at 4°C, then loaded on a Suc density gradient obtained by freezing and thawing 0.5 M Suc, 20 mM Tricine-NaOH (pH 7.8), and 0.05% β-DDM (w/v) and centrifuged for 17 h at 240,000*g* at 4°C.

Clear-native gels (1 mm) were prepared and run as previously described (Järvi et al., 2011) with the addition of 0.3% (w/v) sodium deoxycholate (Sigma) to the Suc band samples. PSI-LHCI and PSI core from Arabidopsis were prepared as reported previously (Wientjes et al., 2011). Tricine (14% [w/v]) SDS-PAGE gels were prepared and run as reported previously (Schägger, 2006).

Steady-State Spectroscopy

The sample buffer used for all room temperature experiments was 0.5 M Suc, 20 mM Tricine (pH 7.8), and 0.05% β-DDM (w/v). In addition, for the 77 K experiments, the buffer contained 66% (w/w) glycerol. Sample OD at the maximum in the red region of the spectrum was adjusted between 0.8 and 1 for absorption and below 0.05 for fluorescence measurements. Absorption spectra were recorded with a Cary 4000 spectrophotometer (Varian). For 77 K measurements samples were cooled in a cryostat (Oxford Instruments). The 77 K absorption spectra were measured with a UV-2600 spectrophotometer (Shimadzu). Fluorescence emission spectra were recorded on a Fluorlog 3.22 spectrofluorimeter (Jobin-Yvon). For fluorescence emission spectra, the spectral bandwidths were 3 nm for excitation (440, 475, and 500 nm), and 1 nm for emission. An optical filter was placed before the detection path to block light <600 nm.

Pigment Analyses

PSI complexes from eight pooled CNBs were eluted overnight in 10 mM Tricine-NaOH (pH 7.8) with 0.05% (w/v) β-DDM and then concentrated in concentrators with a 3 kD cutoff (Amicon Ultra, Millipore) at 7,500*g*. Pigments from Suc bands and eluted CNBs were extracted in 80% (v/v) acetone and analyzed by HPLC (System Gold 126, Beckman Coulter) with the previously described protocol (van den Berg et al., 2018).

Functional Antenna Size

The rate of P_{700} oxidation that is directly proportional to the absorption cross section was measured directly on multiple pooled CNBs and in a separate experiment on thylakoids, both with similar, low optical density at 630 nm to avoid concentration-induced shading. A JTS-10 spectrometer was used (BioLogic) and absorption changes were monitored at 705 nm with a 10 mm interference filter (10 nm full width at half-maximum; Schott). Detecting light was filtered by 3-mm-thick Schott RG695 glass filters, while

Downloaded on December 10, 2020. - Published by https://plantphysiol.org
Copyright (c) 2020 American Society of Plant Biologists. All rights reserved.

actinic light (light-emitting diodes peaking at 630 nm, ~60 μmol photons m^{-2} s^{-1}) was turned off for ~300 μs during each detection to avoid artifacts. The gel pieces were incubated for 30 min in a solution containing 1 mM methyl viologen (Sigma) to prevent acceptor-side limitations, and 4 mM sodium ascorbate to prevent donor-side limitations. It was systematically verified that the rate of oxidation was at least one order of magnitude faster than the rate of P_{700}^{+} reduction and, conversely, that the reduction proceeded to completion between illuminations and an identical quantity of P_{700}^{+} was reached upon each oxidation.

The rates of P_{700} oxidation in *B. braunii* were compared with that of known complexes of Arabidopsis (Wientjes et al., 2009). Curves were minimum-maximum normalized before averaging and fitting. The rates were fitted with monoexponential function in OriginLab software. The measurements were averaged three to six times and performed on two independent CN gels; thylakoids were measured five times on two independent preparations.

Single-Particle Analyses

Multiple CNB1-containing PSI-LHCI supercomplexes were excised and placed in an Eppendorf tube with 60 μL of buffer (10 mM tricine-NaOH, 0.05% [w/v] β-DDM [pH 7.8]) at 4°C overnight with continuous stirring (Kouřil et al., 2014). Spontaneously eluted samples were used for the preparation of EM specimens by negative staining using 2% (w/v) uranyl acetate on glow-discharged carbon-coated copper grids. Approximately 7,300 images were collected using semi-automated GRACE software (Oostergetel et al., 1998) on a FEI Technai T20 microscope equipped with a LaB6 cathode, operating at 200 kV. Images of 2,048 × 2,048 pixels were recorded at 133.000× magnification using a Gatan 4000 SP 4 K slow-scan charge-coupled device camera with a pixel size of 0.224 nm. From the selected EM micrographs, >55,800 particles (top-view PSI) were picked for single-particle analysis using the SCIPION image processing framework (de la Rosa-Trevín et al., 2016).

Time-Resolved Fluorescence

Picosecond time-resolved fluorescence measurements were performed with a streak camera setup as described previously (Le Quiniou et al., 2015a). Samples were placed in 10 mM Tricine (pH 7.8), 0.05% (w/v) β-DDM, and 0.5 M Suc at an optical density (OD) at 679 nm of 1.2 and measured in a 10 × 10-mm quartz cuvette (Hellma Analytics) at room temperture. During the measurements, the sample was stirred with a magnet bar (1,500 rpm). To minimize reabsorption, the laser beam (400 or 475 nm) was focused on the sample close to the cuvette wall and emission was collected at the right angle. To avoid singlet-singlet annihilation, the pulse energy was reduced to 0.4 to 0.6 nJ (100 μW [400 nm] or 140 μW [475 nm] measured at the sample position). A power study confirmed the absence of annihilation (Supplemental Fig. S5). Colonies were measured in fresh culture media with 20 μM DCMU (Sigma) and 1 mM HA (Sigma) at an OD at 679 nm of 0.5 and a pulse energy of 0.13 nJ. Fluorescence was detected from 590 to 860 nm and 0 to 155 ps (time range [TR] 1; temporal response, 4–5 ps) and 0 to 1,500 ps (TR4; temporal response, 18 ps), and each dataset consisted of a sequence of images: 400 images of 10 s at TR1 and 100 images of 1 min at TR4. Image sequences were corrected for background, shading, and jitter (temporal drift between images within an image sequence) and finally averaged in HPD-TA 8.4.0 (Hamamatsu). These corrected datasets were binned to 2 nm, and zoomed between 640 and 800 nm in Glotaran 1.3 (Snellenburg et al., 2012). The datasets were analyzed globally with a sequential model in order to extract a minimum number of exponential components, n (with increasing lifetimes τn), that can satisfactorily describe the data (van Stokkum et al., 2004). The instrument response function was modeled as a gaussian with a full width at half-maximum of 4 ps (TR1) or 26 ps (TR4). Average lifetimes were calculated as $\Sigma(A^{*}\tau)/\Sigma A$, with amplitude A taken as the area of the DAS over the 640 to 800 nm interval.

Supplemental Data

The following supplemental materials are available.

Supplemental Table S1. Overview of homologous protein sequences detected in the *B. braunii* genome with query sequences from Arabidopsis and *C. reinhardtii*.

Supplemental Figure S2. Projection maps of *B. braunii* PSI-LHCI, obtained by single-particle electron microscopy.

Supplemental Figure S3. Structural models of two less abundant classes of PSI-LHCI supercomplexes isolated from *B. braunii*.

Supplemental Figure S4. Functional antenna size of PSI in *B. braunii* thylakoids compared to Arabidopsis thylakoids.

Supplemental Figure S5. Time-resolved fluorescence measurements of the PSI-LHCI complex isolated from *B. braunii* measured with a streak camera.

ACKNOWLEDGMENTS

Dr. Lijin Tian is acknowledged for his kind advice regarding the streak camera measurements. Maurits Dijkstra is acknowledged for his help with similarity search in the *B. braunii* genome.

Received June 22, 2020; accepted September 28, 2020; published October 13, 2020.

LITERATURE CITED

Alboresi A, Le Quiniou C, Yadav SKN, Scholz M, Meneghesso A, Gerotto C, Simionato D, Hippler M, Boekema EJ, Croce R, et al (2017) Conservation of core complex subunits shaped the structure and function of photosystem I in the secondary endosymbiont alga *Nannochloropsis gaditana*. New Phytol **213:** 714–726

Anderson JM, Chow WS, Park YI (1995) The grand design of photosynthesis: Acclimation of the photosynthetic apparatus to environmental cues. Photosynth Res **46:** 129–139

Ballottari M, Dall'Osto L, Morosinotto T, Bassi R (2007) Contrasting behavior of higher plant photosystem I and II antenna systems during acclimation. J Biol Chem **282:** 8947–8958

Beardall J, Allen D, Bragg J, Finkel ZV, Flynn KJ, Quigg A, Rees TAV, Richardson A, Raven JA (2009) Allometry and stoichiometry of unicellular, colonial and multicellular phytoplankton. New Phytol **181:** 295–309

Benson SL, Maheswaran P, Ware MA, Hunter CN, Horton P, Jansson S, Ruban AV, Johnson MP (2015) An intact light harvesting complex I antenna system is required for complete state transitions in *Arabidopsis*. Nat Plants **1:** 15176

Bos I, Bland KM, Tian L, Croce R, Frankel LK, Amerongen H Van, Bricker TM, Wientjes E (2017) Multiple LHCII antennae can transfer energy ef fi ciently to a single photosystem I. Biochimt Biophys Acta **1858:** 371–378

Browne DR, Jenkins J, Schmutz J, Shu S, Barry K, Grimwood J, Chiniquy J, Sharma A, Niehaus TD, Weiss TL, et al (2017) Draft nuclear genome sequence of the liquid hydrocarbon-accumulating green microalga *Botryococcus braunii* race B (Showa). Genome Announc **5:** e00215-17

Busch A, Hippler M (2011) The structure and function of eukaryotic photosystem I. Biochim Biophys Acta **1807:** 864–877

Carbonera D, Agostini G, Morosinotto T, Bassi R (2005) Quenching of chlorophyll triplet states by carotenoids in reconstituted Lhca4 subunit of peripheral light-harvesting complex of photosystem I. Biochemistry **44:** 8337–8346

Chukhutsina VU, Holzwarth AR, Croce R (2019) Time-resolved fluorescence measurements on leaves: Principles and recent developments. Photosynth Res **140:** 355–369

Chukhutsina VU, Liu X, Xu P, Croce R (2020) Light-harvesting complex II is an antenna of photosystem I in dark-adapted plants. Nat Plants **6:** 860–868

Croce R, Morosinotto T, Castelletti S, Breton J, Bassi R (2002) The Lhca antenna complexes of higher plants photosystem I. Biochim Biophys Acta **1556:** 29–40

Croce R, van Amerongen H (2020) Light harvesting in oxygenic photosynthesis: Structural biology meets spectroscopy. Science **369:** eaay2058

Croce R, van Amerongen H (2013) Light-harvesting in photosystem I. Photosynth Res **116:** 153–166

de la Rosa-Trevín JM, Quintana A, Del Cano L, Zaldívar A, Foche I, Gutiérrez J, Gómez-Blanco J, Burguet-Castell J, Cuenca-Alba J, Abrishami V, et al (2016) Scipion: A software framework toward integration, reproducibility and validation in 3D electron microscopy. J Struct Biol **195:** 93–99

Downloaded on December 10, 2020. - Published by https://plantphysiol.org
Copyright (c) 2020 American Society of Plant Biologists. All rights reserved.

Drop B, Webber-Birungi M, Fusetti F, Kouřil R, Redding KE, Boekema EJ, Croce R (2011) Photosystem I of *Chlamydomonas reinhardtii* contains nine light-harvesting complexes (Lhca) located on one side of the core. J Biol Chem **286:** 44878–44887

Drop B, Yadav K N S, Boekema EJ, Croce R (2014) Consequences of state transitions on the structural and functional organization of photosystem I in the green alga *Chlamydomonas reinhardtii*. Plant J **78:** 181–191

Engelmann E, Zucchelli G, Casazza AP, Brogioli D, Garlaschi FM, Jennings RC (2006) Influence of the photosystem I-light harvesting complex I antenna domains on fluorescence decay. Biochemistry **45:** 6947–6955

Eroglu E, Okada S, Melis A (2011) Hydrocarbon productivities in different *Botryococcus* strains: Comparative methods in product quantification. J Appl Phycol **23:** 763–775

García-Cubero R, Cabanelas ITD, Sijtsma L, Kleinegris DMM, Barbosa MJ (2018) Production of exopolysaccharide by *Botryococcus braunii* CCALA 778 under laboratory simulated Mediterranean climate conditions. Algal Res **29:** 330–336

Gobets B, Kennis JTM, Ihalainen JA, Brazzoli M, Croce R, Van Stokkum IHM, Bassi R, Dekker JP, Van Amerongen H, Fleming GR, et al (2001) Excitation energy transfer in dimeric light harvesting complex I: A combined streak-camera/fluorescence upconversion study. J Phys Chem B **105:** 10132–10139

Gouveia JD, Ruiz J, van den Broek LAM, Hesselink T, Peters S, Kleinegris DMM, Smith AG, van der Veen D, Barbosa MJ, Wijffels RH (2017) *Botryococcus braunii* strains compared for biomass productivity, hydrocarbon and carbohydrate content. J Biotechnol **248:** 77–86

Grotjohann I, Fromme P (2013) Photosystem I. In W Lennarz, and M Lane, eds, Ed 2. Encyclopedia of Biological Chemistry, New York, pp 503–507

Iwai M, Grob P, Iavarone AT, Nogales E, Niyogi KK (2018) A unique supramolecular organization of photosystem I in the moss *Physcomitrella patens*. Nat Plants **4:** 904–909

Iwai M, Yokono M (2017) Light-harvesting antenna complexes in the moss *Physcomitrella patens*: Implications for the evolutionary transition from green algae to land plants. Curr Opin Plant Biol **37:** 94–101

Järvi S, Suorsa M, Paakkarinen V, Aro E-M (2011) Optimized native gel systems for separation of thylakoid protein complexes: Novel super- and mega-complexes. Biochem J **439:** 207–214

Jennings RC, Zucchelli G, Croce R, Garlaschi FM (2003) The photochemical trapping rate from red spectral states in PSI-LHCI is determined by thermal activation of energy transfer to bulk chlorophylls. Biochim Biophys Acta **1557:** 91–98

Kouřil R, Strouhal O, Nosek L, Lenobel R, Chamrád I, Boekema EJ, Šebela M, Ilík P (2014) Structural characterization of a plant photosystem I and NAD(P)H dehydrogenase supercomplex. Plant J **77:** 568–576

Kubota-Kawai H, Burton-Smith RN, Tokutsu R, Song C, Akimoto S, Yokono M, Ueno Y, Kim E, Watanabe A, Murata K, et al (2019) Ten antenna proteins are associated with the core in the supramolecular organization of the photosystem I supercomplex in *Chlamydomonas reinhardtii*. J Biol Chem **294:** 4304–4314

Kyle DJ, Staehelin LA, Arntzen CJ (1983) Lateral mobility of the light-harvesting complex in chloroplast membranes controls excitation energy distribution in higher plants. Arch Biochem Biophys **222:** 527–541

Le Quiniou C, Tian L, Drop B, Wientjes E, van Stokkum IHM, van Oort B, Croce R (2015b) PSI-LHCI of *Chlamydomonas reinhardtii*: Increasing the absorption cross section without losing efficiency. Biochim Biophys Acta **1847:** 458–467

Le Quiniou C, van Oort B, Drop B, van Stokkum IHM, Croce R (2015a) The high efficiency of photosystem I in the green alga *Chlamydomonas reinhardtii* is maintained after the antenna size is substantially increased by the association of light-harvesting complexes II. J Biol Chem **290:** 30587–30595

Mazor Y, Borovikova A, Caspy I, Nelson N (2017) Structure of the plant photosystem I supercomplex at 2.6 Å resolution. Nat Plants **3:** 17014

Metzger P, Largeau C (2005) *Botryococcus braunii*: A rich source for hydrocarbons and related ether lipids. Appl Microbiol Biotechnol **66:** 486–496

Moseley JL, Allinger T, Herzog S, Hoerth P, Wehinger E, Merchant S, Hippler M (2002) Adaptation to Fe-deficiency requires remodeling of the photosynthetic apparatus. EMBO J **21:** 6709–6720

Mozzo M, Mantelli M, Passarini F, Caffarri S, Croce R, Bassi R (2010) Functional analysis of Photosystem I light-harvesting complexes (Lhca) gene products of *Chlamydomonas reinhardtii*. Biochim Biophys Acta **1797:** 212–221

Nawrocki WJ, Santabarbara S, Mosebach L, Wollman FA, Rappaport F (2016) State transitions redistribute rather than dissipate energy between the two photosystems in *Chlamydomonas*. Nat Plants **2:** 16031

Neilson JAD, Durnford DG (2010) Structural and functional diversification of the light-harvesting complexes in photosynthetic eukaryotes. Photosynth Res **106:** 57–71

Oostergetel GT, Keegstra W, Brisson A (1998) Automation of specimen selection and data acquisition for protein electron crystallography. Ultramicroscopy **74:** 47–59

Ozawa S-I, Bald T, Onishi T, Xue H, Matsumura T, Kubo R, Takahashi H, Hippler M, Takahashi Y (2018) Configuration of ten light-harvesting chlorophyll *a*/*b* complex I subunits in *Chlamydomonas reinhardtii* photosystem I. Plant Physiol **178:** 583–595

Pan X, Su X, Cao P, Chang W, Liu Z, Zhang X, Li M (2018) Structure of the maize photosystem I supercomplex with light-harvesting complexes I and II. Science **1113:** 1109–1113

Pi X, Tian L, Dai H-E, Qin X, Cheng L, Kuang T, Sui S-F, Shen J-R (2018) Unique organization of photosystem I-light-harvesting supercomplex revealed by cryo-EM from a red alga. Proc Natl Acad Sci USA **115:** 4423–4428

Pietrzykowska M, Suorsa M, Semchonok DA, Tikkanen M, Boekema EJ, Aro E-M, Jansson S (2014) The light-harvesting chlorophyll *a*/*b* binding proteins Lhcb1 and Lhcb2 play complementary roles during state transitions in *Arabidopsis*. Plant Cell **26:** 3646–3660

Pinnola A, Alboresi A, Nosek L, Semchonok D, Rameez A, Trotta A, Barozzi F, Kouřil R, Dall'Osto L, Aro E-M, et al (2018) A LHCB9-dependent photosystem I megacomplex induced under low light in *Physcomitrella patens*. Nat Plants **4:** 910–919

Qin X, Pi X, Wang W, Han G, Zhu L, Liu M, Cheng L, Shen JR, Kuang T, Sui SF (2019) Structure of a green algal photosystem I in complex with a large number of light-harvesting complex I subunits. Nat Plants **5:** 263–272

Rivadossi A, Zucchelli G, Garlaschi FM, Jennings RC (1999) The importance of PS I chlorophyll red forms in light-harvesting by leaves. Photosynth Res **60:** 209–215

Romero E, Mozzo M, van Stokkum IHM, Dekker JP, van Grondelle R, Croce R (2009) The origin of the low-energy form of photosystem I light-harvesting complex Lhca4: Mixing of the lowest exciton with a charge-transfer state. Biophys J **96:** L35–L37

Schägger H (2006) Tricine—SDS-PAGE. Nat Protoc **1:** 16–23

Shen L, Huang Z, Chang S, Wang W, Wang J, Kuang T, Han G, Shen JR, Zhang X (2019) Structure of a $C_2S_2M_2N_2$-type PSII-LHCII supercomplex from the green alga *Chlamydomonas reinhardtii*. Proc Natl Acad Sci USA **116:** 21246–21255

Snellenburg JJ, Laptenok SP, Seger R, Mullen KM, van Stokkum IHM (2012) Glotaran : A Java-based graphical user interface for the R package TIMP. J Stat Softw **49:** 1–22

Su X, Ma J, Pan X, Zhao X, Chang W, Liu Z, Zhang X, Li M (2019) Antenna arrangement and energy transfer pathways of a green algal photosystem-I-LHCI supercomplex. Nat Plants **5:** 273–281

Su X, Wei X, Zhu D, Chang W, Liu Z, Zhang X, Li M (2017) Structure and assembly mechanism of plant C2S2M2-type PSII-LHCII supercomplex. Science **820:** 815–820

Suga M, Ozawa S-I, Yoshida-Motomura K, Akita F, Miyazaki N, Takahashi Y (2019) Structure of the green algal photosystem I supercomplex with a decameric light-harvesting complex I. Nat Plants **5:** 626–636

Suga M, Shen JR (2020) Structural variations of photosystem I-antenna supercomplex in response to adaptations to different light environments. Curr Opin Struct Biol **63:** 10–17

Swingley WD, Iwai M, Chen Y, Ozawa S-I, Takizawa K, Takahashi Y, Minagawa J (2010) Characterization of photosystem I antenna proteins in the prasinophyte *Ostreococcus tauri*. Biochim Biophys Acta **1797:** 1458–1464

Tasić MB, Pinto LFR, Klein BC, Veljković VB, Filho RM (2016) *Botryococcus braunii* for biodiesel production. Renew Sustain Energy Rev **64:** 260–270

van den Berg TE, Chukhutsina VU, van Amerongen H, Croce R, van Oort B (2019) Light acclimation of the colonial green alga *Botryococcus braunii* strain Showa. Plant Physiol **179:** 1132–1143

Downloaded on December 10, 2020. - Published by https://plantphysiol.org
Copyright (c) 2020 American Society of Plant Biologists. All rights reserved.

van den Berg TE, van Oort B, Croce R (2018) Light-harvesting complexes of *Botryococcus braunii*. Photosynth Res **135:** 191–201

van Stokkum IHM, Larsen DS, van Grondelle R (2004) Global and target analysis of time-resolved spectra. Biochim Biophys Acta **1657:** 82–104

Varsano T, Wolf SG, Pick U (2006) A chlorophyll *a*/*b*-binding protein homolog that is induced by iron deficiency is associated with enlarged photosystem I units in the eucaryotic alga *Dunaliella salina*. J Biol Chem **281:** 10305–10315

Wake L, Hillen L (1980) Study of a "bloom" of the oil-rich alga *Botryococcus braunii* in the Darwin River Reservoir. Biotechnol Bioeng **XXII:** 1637–1656

Watanabe M, Semchonok DA, Webber-Birungi MT, Ehira S, Kondo K, Narikawa R, Ohmori M, Boekema EJ, Ikeuchi M (2014) Attachment of phycobilisomes in an antenna-photosystem I supercomplex of cyanobacteria. Proc Natl Acad Sci USA **111:** 2512–2517

Wientjes E, Oostergetel GT, Jansson S, Boekema EJ, Croce R (2009) The role of Lhca complexes in the supramolecular organization of higher plant photosystem I. J Biol Chem **284:** 7803–7810

Wientjes E, van Amerongen H, Croce R (2013a) LHCII is an antenna of both photosystems after long-term acclimation. Biochim Biophys Acta **1827:** 420–426

Wientjes E, van Amerongen H, Croce R (2013b) Quantum yield of charge separation in photosystem II: Functional effect of changes in the antenna size upon light acclimation. J Phys Chem B **117:** 11200–11208

Wientjes E, van Stokkum IHM, van Amerongen H, Croce R (2011) The role of the individual Lhcas in photosystem I excitation energy trapping. Biophys J **101:** 745–754

Downloaded on December 10, 2020. - Published by https://plantphysiol.org
Copyright (c) 2020 American Society of Plant Biologists. All rights reserved.